

# Resonance blocking and passing effects in two-dimensional elastic waveguides with obstacles

Evgeny Glushkov,<sup>a)</sup> Natalia Glushkova, Mikhail Golub, and Artem Eremin

*Institute for Mathematics, Mechanics and Informatics, Kuban State University, Krasnodar, 350040, Russia*

(Received 13 September 2010; revised 26 February 2011; accepted 26 April 2011)

Resonance localization of wave energy in two-dimensional (2D) waveguides with obstacles, known as a trapped mode effect, results in blocking of wave propagation. This effect is closely connected with the allocation of natural resonance poles in the complex frequency plane, which are in fact the spectral points of the related boundary value problem. With several obstacles the number of poles increases in parallel with the number of defects. The location of the poles in the complex frequency plane depends on the defect's relative position, but the gaps of transmission coefficient plots generally remain in the same frequency ranges as for every single obstacle separately. This property gives a possibility to extend gap bands by a properly selected combination of various scatterers. On the other hand, a resonance wave passing in narrow bands associated with the poles is also observed. Thus, while a resonance response of a single obstacle works as a blocker, the waveguide with several obstacles becomes opened in narrow vicinities of nearly real spectral poles, just as it is known for one-dimensional (1D) waveguides with a finite number of periodic scatterers. In the present paper the blocking and passing effects are analyzed based on a semi-analytical model for wave propagation in a 2D elastic layer with cracks or rigid inclusions.

© 2011 Acoustical Society of America. [DOI: 10.1121/1.3592225]

PACS number(s): 43.35.Cg, 43.20.Bi, 43.20.Gp, 43.20.Ks [ANN]

Pages: 113–121

## I. INTRODUCTION

The effect of traveling wave blocking by a system of obstacles is widely used in various areas, such as vibrodamping, anti-seismic protection, opto- and microelectronics, etc. The effect manifests itself as deep gaps in the frequency spectra of transmitted signals. The gap band appearance is especially sound in periodic structures, e.g., with systems of interdigital contacts or grooves used in acoustoelectronic technology, in periodic composites, phononic lattices, and photonic crystals. The Bloch-Floquet theory provides exhaustive information about wave processes in infinite periodic structures,<sup>1</sup> however, it becomes inapplicable with a finite number of scatterers or if a fluctuation in cell properties occurs. Numerical examples for disordered phononic<sup>2</sup> and photonic crystals<sup>3,4</sup> show that even a little deviation may considerably change their transmitting and blocking properties.

On the other hand, a resonant shielding of traveling waves by one or more obstacles is known as a trapped mode effect.<sup>5,6</sup> This effect features the capture and localization of time-averaged wave energy of a time-harmonic wave field  $\mathbf{u}e^{-i\omega t}$  in the form of energy vortices.<sup>7</sup> The trapped mode effect is closely connected with the allocation of spectral points  $\omega_n$  of the corresponding boundary value problem. They appear in the solution as complex poles of the frequency spectrum of the diffracted field  $\mathbf{u}_{sc}$  analytically continued into the complex frequency plane  $\omega$ . The points  $\omega_n$  are natural frequencies of the waveguide with obstacles. The closer a pole  $\omega_n$  is located to the real axis, the more the

trapped mode effect becomes apparent at  $\omega_g \approx \text{Re}\omega_n$ . Specific forms of energy localization are governed by the eigen-solutions  $\mathbf{u}_n$  associated with the spectral points  $\omega_n$ .

Besides the blocking ability, the resonance response of hidden defects can be used for nondestructive testing purposes, e.g., for guided wave crack detection in plates and composite laminates. Therefore, two-dimensional (2D) elastic layer waveguides with defects in the form of cracks, voids, and inclusions are also in the focus of research. Our studies have shown that with several defects the eddies of wave energy may work not only as blockers but also as energy pumps. It has been ascertained that accounting for mutual wave interplay among the obstacles leads to a realignment of energy streamlines in such a way that the energy circulation in the vortex zones formed around the obstacles becomes coordinated, providing energy passage. In the transmission coefficient plots  $\kappa^+(\omega)$  such pass modes appear as narrow peaks centered at frequencies  $\omega_p$  located close to the resonance poles  $\omega_n$ :  $\omega_p \approx \text{Re}\omega_n$ , just as in the case of one-dimensional (1D) waveguide structures.<sup>8</sup> The number of poles  $\omega_n$  and, correspondingly, of the transmission peaks is proportional to the number of obstacles  $M$  so that with a large  $M$  the plots  $\kappa^+(\omega)$  exhibit typical comb-like patterns. It is significant that such transmission peak patterns, as well as the patterns of nearly real pole groups, are inherent to a wide variety of physically different 1D waveguides.<sup>3,8–12</sup> As  $M$  increases, the peaks tightly fill in restricted frequency intervals forming pass bands inside wider gap bands in compliance with the Bloch-Floquet theory.

The present paper aims at the description of similar effects revealed for 2D structures, specified in Sec. II. To gain a coherent understanding, we start from blocking effects

<sup>a)</sup>Author to whom correspondence should be addressed. Electronic mail: evg@math.kubsu.ru

peculiar to one-defect waveguides (Sec. III). Then the appearance of resonance pass peaks in the case of two and more obstacles is shown in Sec. IV. These examples are augmented by the examples for a 1D model of a spring supported string with pointwise defects,<sup>12</sup> intended to visually illustrate the connection between the allocation of pass peaks and resonance poles.

## II. MATHEMATICAL FRAMEWORK

Time-harmonic guided wave propagation in a 2D elastic layer with thin or volumetric defects (Fig. 1) is described by the displacement field  $\mathbf{u}(\mathbf{x}, \omega)e^{-i\omega t}$ ,  $\mathbf{u} = (u_x, u_z)$ ,  $x = (x, z)$ , formed from the incident and scattered fields  $\mathbf{u}_0$  and  $\mathbf{u}_{sc}$ :  $\mathbf{u} = \mathbf{u}_0 + \mathbf{u}_{sc}$ . The incident field  $\mathbf{u}_0$  generated by a surface load  $\mathbf{q}$  obeys the elastodynamic Lamé-Navier equations and boundary conditions at the plane-parallel sides of the waveguide without obstacles. It can be represented via the convolution of the Green matrix  $k$  with the source vector  $\mathbf{q}$ :  $\mathbf{u}_0 = k * \mathbf{q}$ .<sup>7,13</sup>

Furthermore, the incident field in the form of traveling waves  $\mathbf{u}_0 = \sum_j \mathbf{a}_j(z)e^{i\zeta_j x}$  is derived from the integral representation using the residue technique. In this context, the wave numbers  $\zeta_j$  are poles of the Green matrix Fourier symbol  $K(\alpha, z) = \mathcal{F}_x[k(x, z)]$  in the complex  $\alpha$ -plane ( $\alpha$  is the parameter of the Fourier transform  $\mathcal{F}_x$  with respect to the longitudinal coordinate  $x$ ); the amplitude vectors  $\mathbf{a}_j$  are expressed through the residues of  $K$  at these poles. Specific forms of the Green matrix elements and of the incoming Lamb modes may be found in Ref. 7.

Outside the obstacle domain  $\Omega = \cup_m \Omega_m$ , the scattered field  $\mathbf{u}_{sc}$  satisfies the same governing equations and boundary conditions as  $\mathbf{u}_0$ , hence, it is also representable via the waveguide Green matrix and, further, in terms of propagating and inhomogeneous modes associated with the real and complex  $\zeta_j$ , respectively. Such representations include unknown factors that have to be fixed via solution of the corresponding diffraction problem. In general, the latter can be reduced to a

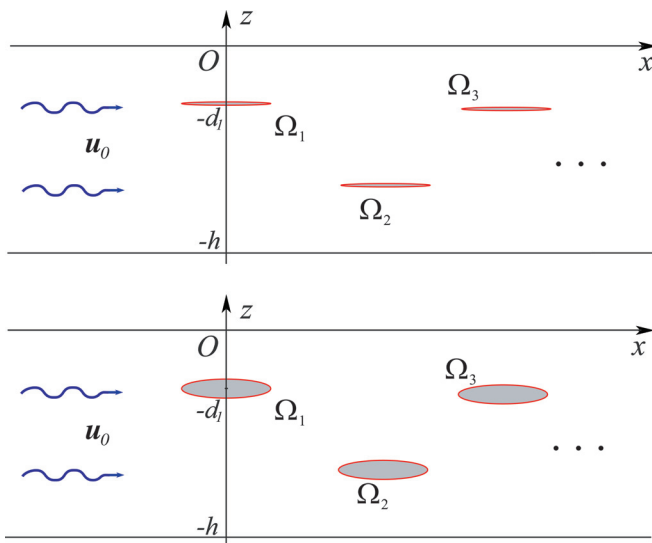


FIG. 1. (Color online) Elastic waveguides with thin and volumetric obstacles.

boundary integral equation (BIE) with respect to an unknown vector function set on the obstacle boundary  $S$  ( $S = \partial\Omega$ ). In the case of cracks or thin inclusions the BIE is discretized by expanding the unknown vector function in terms of splines or orthogonal polynomials.<sup>7,13</sup> For volumetric voids and inclusions the discretization is based on the laminate element approximation.<sup>14</sup> In all cases the problem is reduced to a linear algebraic system

$$A\mathbf{c} = \mathbf{f} \quad (1)$$

with respect to the vector of unknown expansion coefficients  $\mathbf{c} = (c_1, c_2, \dots, c_N)^T$ . The roots of the characteristic equation

$$\Delta(\omega) \equiv \det A(\omega) = 0 \quad (2)$$

approximate spectral points  $\omega_n$  of the diffraction problem. In fact,  $\omega_n$  are poles of the diffracted field  $\mathbf{u}_{sc}(\mathbf{x}, \omega)$  considered as a function of  $\omega$  analytically continued into the complex  $\omega$ -plane.

The transport of wave energy in the time-harmonic field  $\mathbf{u}e^{-i\omega t}$  is visualized by the energy streamlines, which show the trajectories of time-averaged energy fluxes. At every point  $\mathbf{x}$  they are tangential to the power density vector  $\mathbf{e} = (e_x, e_z) = (e_1, e_2)$  introduced by N. Umov for elastodynamic fields as far back as the 19th century.<sup>15</sup> Its components  $e_n$  are expressed via the displacement and stress vectors  $\mathbf{u}$  and  $\boldsymbol{\tau}_n$ :  $e_n = -\frac{\omega}{2} \text{Im}(\mathbf{u}, \boldsymbol{\tau}_n)$  ( $\boldsymbol{\tau}_n$  is a stress vector at an elementary area orthogonal to the  $n$ -th coordinate axis). The integration of the horizontal component  $e_x$  over the layer cross section yields the total amount of time-averaged energy carried by elastic waves along the waveguide:  $E = \int_{-h}^0 e_x dz$ . The transmission coefficient  $\kappa^+ = E/E_0$  is introduced as the ratio of the energy  $E$  carried by the total field  $\mathbf{u} = \mathbf{u}_0 + \mathbf{u}_{sc}$  behind the obstacles to the energy  $E_0$  carried by the incident field  $\mathbf{u}_0$ .

Hereinafter, the numerical examples are given in the dimensionless form assuming the layer thickness  $h$ , the shear wave velocity  $c_s$  and the density  $\rho$  to be units; Poisson's ratio  $\nu = 1/3$ . The dimensionless angular frequency  $\omega = 2\pi fh/c_s$ , where  $f$  is dimensional frequency. The waveguide occupies the domain  $-\infty < x < \infty$ ,  $-1 \leq z \leq 0$ .

## III. ONE DEFECT CASE

In the elastic layer with one crack the trapped mode effect occurs at frequencies  $\omega_g \approx \text{Re}\omega_n$ , where the poles  $\omega_n$  are located close to the real axis ( $|\text{Im}\omega_n/\text{Re}\omega_n| \ll 1$ ). With a totally real  $\omega_n$  (which is rather seldom in the problems considered) the residue  $\text{res } \mathbf{u}_{sc}(\mathbf{x}, \omega)|_{\omega=\omega_n}$  is an eigenform of the oscillation  $e^{-i\omega_n t}$  of the defected waveguide. Usually it exhibits strong localization of the oscillation amplitude near the obstacles, indicating the accumulation of wave energy in energy vortices.<sup>7</sup> Such vortices block up the energy flow transferred along the waveguide by the incident field  $\mathbf{u}_0$ .

Figure 2 gives examples of energy streamlines and power density distribution in the case of resonant (top) and nonresonant (bottom) waveguide blocking by a single horizontal obstacle. In the first case the obstacle is a strip-like

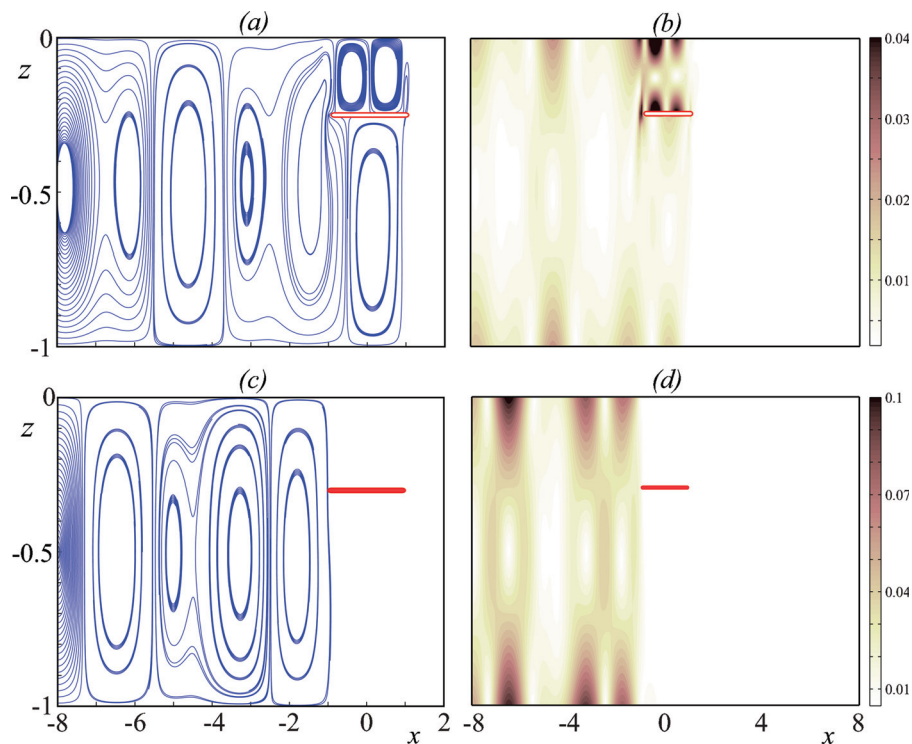


FIG. 2. (Color online) Energy streamlines [(a), (c)] and power density  $|e(x,z)|$  [(b), (d)] in the case of resonant (top) and nonresonant (bottom) blocking of incoming  $A_0$  mode by a strip-like crack and a thin rigid inclusion, respectively.

crack of half-length  $l=1$  and depth  $d=0.25$ . It is modeled by an infinitesimally thin cut with stress-free sides:  $\tau|_S = 0$  ( $\tau$  is a stress vector at a horizontal surface element). At the bottom subplots the defect is a thin rigid inclusion ( $l=1$ ,  $d=0.3$ ), which is assumed to be immovable ( $\mathbf{u}|_S = 0$ ). The wave field is induced by the  $A_0$  mode incidence at  $\omega = 1.31$ , which is resonance frequency for the crack but nonresonance for the inclusion.

In the first case [Fig. 2(a)], the resonant vortices with high density of circulating energy [dark spots in Fig. 2(b)] appear between the crack and the nearest layer side (see also Ref. 7). In the second case, nonresonant wave shielding is featured by the absence of such energy vortices with high energy concentration [Figs. 2(c) and 2(d)]. There are no resonance poles  $\omega_n$  nearby the frequency  $\omega = 1.31$ , and the blocking is physically explained by the fact that no traveling waves may exist in the local waveguides above and beneath the inclusion since they are one-clamped-side waveguides. Indeed, the first dimensionless cut-off frequency of a free-fixed elastic layer of unit thickness is  $\omega_1^* = \pi/2$ , hence the cut-off frequencies of those local waveguides of thicknesses  $d$  and  $1-d$  are  $\omega_1^*/d \approx 5.23$  and  $\omega_1^*/(1-d) \approx 2.24$ , which is higher than the frequency  $\omega = 1.31$  considered.

The resonant and nonresonant blocking effects appear in the plots of the transmission coefficient  $\kappa^+(\omega)$  in basically different ways (Fig. 3). One can see that in the first subplot the resonance frequency  $\omega_g = 1.31$ , marked by the arrow, is featured by a deep gap connected with the wave transmission shielding by the energy vortices shown in Fig. 2(a). On the contrary, no gap is observed at this frequency in the second subplot, which illustrates nonresonant but very good ( $\kappa^+ < 0.01$ ) blocking in a wide frequency range due to the absence of traveling waves above and beneath the inclusion for  $\omega < 2.24$ .

## IV. WAVEGUIDES WITH TWO AND MORE OBSTACLES

### A. Gap band independence from obstacles' relative position

Because the resonance gap bands were comparatively narrow, we attempted to find a way of their extension by combining several obstacles.<sup>13</sup> Besides, there was an additional question of self-dependent interest: how the poles  $\omega_n$  would be allocated and appear with two and more obstacles. It was felt that the presence of multiple defects might lead to effects contradicting in some respects with the single-defect resonance phenomena above. Indeed, on the one hand, the mutual influence of defects should change the pole distribution in the  $\omega$ -plane. On the other hand, if vortices at the first obstacle have already blocked the propagation of a signal, the presence of the following ones should not affect the

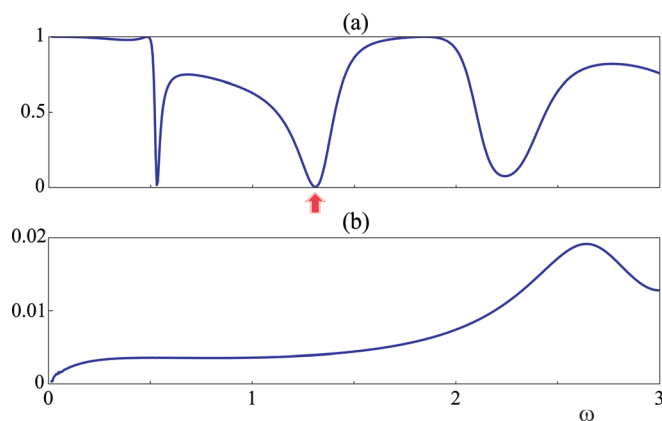


FIG. 3. (Color online) Frequency dependences of the transmission coefficient  $\kappa^+(\omega)$  for the same crack (a) and inclusion (b) as in Fig. 2; the arrow shows  $\omega_g = \text{Re}\omega_n$  for the nearly real resonance pole  $\omega_n$  occurring in the crack case.

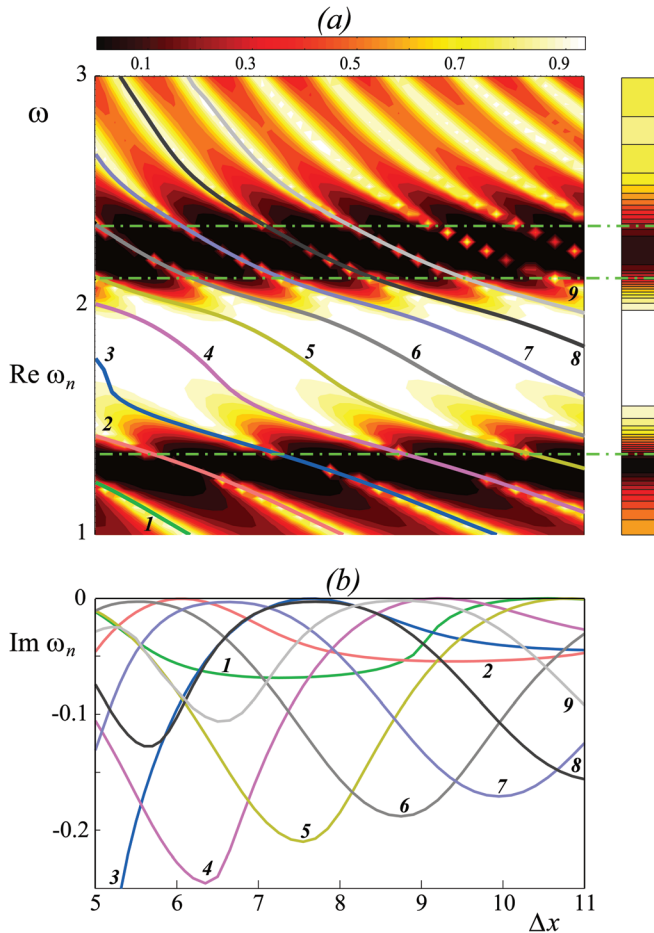


FIG. 4. (Color online) The transmission coefficient  $\kappa^+$  for two cracks as a function of  $\Delta x$  and  $\omega$ , and the resonance poles  $\omega_n$  as functions of  $\Delta x$ .

pattern because the signal does not arrive at them. In other words, additional obstacles screened by the first one should not change the frequency of resonance blocking  $\omega_g$  and, consequently, the location of the corresponding nearly real pole  $\omega_n$ .

Even the first numerical experiments carried out for the elastic layer with two cracks have demonstrated that both these seemingly alternative possibilities took place simultaneously: the location of the poles  $\omega_n$  constantly varied with the horizontal distance  $\Delta x$  between them, but it occurred in such a way that the blocking ranges, conditioned by every single defect separately, remained intact. Figure 4 (copy of Fig. 2 from Ref. 13) illustrates how it may occur. The gray scale pattern shows the transmission coefficient  $\kappa^+$  for the  $A_0$  mode running on two horizontal cracks of unit half-width ( $l=1$ ) located at the identical depth  $d=0.25$ . The coefficient  $\kappa^+(\Delta x, \omega)$  is shown as a function of two variables: the distance  $\Delta x$  between the crack centers (abscissa axis), and the frequency  $\omega$  (ordinate axes). The darkest areas in the  $(\Delta x, \omega)$  plane correspond to total blocking ( $\kappa^+=0$ ), while the white areas correspond to total transmission ( $\kappa^+=1$ ). The solid lines imposed on the pattern show real parts of the resonance poles  $\omega_n$  as functions of the distance:  $\omega = \text{Re}\omega_n(\Delta x)$  (the numbers on the lines correspond to the sub-indices  $n$  of the poles  $\omega_n$ ). The lower subplot (b) depicts the dependencies of the imaginary parts  $\text{Im}\omega_n(\Delta x)$  with the

respective line numbering. For comparison, a narrow strip in the right part of Fig. 4(a) shows the frequency dependence  $\kappa^+(\omega)$  for the same single crack. Its three resonance frequencies  $\omega_g = \text{Re}\omega_n$  (1.31, 2.11, and 2.34 in the case) are plotted as light dash-dotted lines. The frequency ranges of considerable blocking (horizontal dark strips) are located near these values.

In Fig. 4(a) attention is focused on the fact that with any  $\Delta x$  the blocking ranges remain approximately the same as with a single crack, while the pole location varies. With increasing  $\Delta x$  the values  $\text{Re}\omega_n$  monotonically decrease, while the curves  $\text{Im}\omega_n$  are sine-shaped. Being negative, they alternatively increase up to the limit value  $\text{Im}\omega=0$  and decrease down to certain low limits. Thus, the poles move in the low half-plane  $\text{Im}\omega \leq 0$  from right to left alternatively approaching the real axis  $\text{Im}\omega=0$  and going away from it. At certain distances one of the poles touches the real axis, i.e., it becomes totally real causing a classical trapped-mode effect at such a frequency  $\omega = \omega_n$  (the case of real discrete spectral point  $\omega_n$  lying on the continuous spectrum  $\omega > 0$ ).

At first glance this pole behavior contradicts the inference about their role in the blocking effects. However, a more careful analysis shows that the poles approach the real axis only at the aforementioned frequency ranges of blocking by a single crack. Moreover, when a pole starts moving off from the axis, the next one immediately comes up to this band, substituting for the predecessor. In that way, nearly real poles are in constant attendance at the blocking ranges, providing independent of  $\Delta x$  horizontal dark zones observed in Fig. 4(a).

With a group of cracks of different lengths and depths the blocking bands inherent to each of them are joined together. Obviously, in such a case the nearly real poles are also always on duty at all those frequency bands irrespective of the distance among them. This property enables gap-band extension by combining obstacles with supplementing blocking abilities.<sup>13</sup>

## B. Appearance of resonant transmission frequencies

It was noticed that with several obstacles certain narrow pass peaks in  $\kappa^+(\omega)$  plots were present in the extended stop ranges in spite of full overlapping of joined gap bands. In Fig. 4 the corresponding narrow transmission bands are visible as light stripes traversing gray and dark background along the curves  $\text{Re}\omega_n(\Delta x)$ . Such narrow transmission bands inside wider gap ranges appear for various obstacles independently of their form and properties.

For example, with two rigid elliptic inclusions a pass band inside the range of nonresonant blocking is distinguishable in the  $\kappa^+(\omega, d_2)$  grayscale surface as a light narrow stripe at  $\omega \approx 2$  (Fig. 5, left subplot). The ellipses are of semi-axes  $a=0.5$  and  $b=0.1$  and with the fixed center coordinates  $(x_1, z_1) = (0, -0.5)$  and  $x_2 = 2$ , while the depth  $d_2 = |z_2|$  of the second ellipse is varied. The plot  $\kappa^+(\omega)$  (Fig. 5, right bottom subplot), obtained as a cross section of the surface  $\kappa^+(\omega, d_2)$  along the segment  $1.9 < \omega < 2.1$ ,  $d_2 = 0.14$  (marked by a white rectangle in the left subplot), exhibits considerable (more than 30 times) growth in the

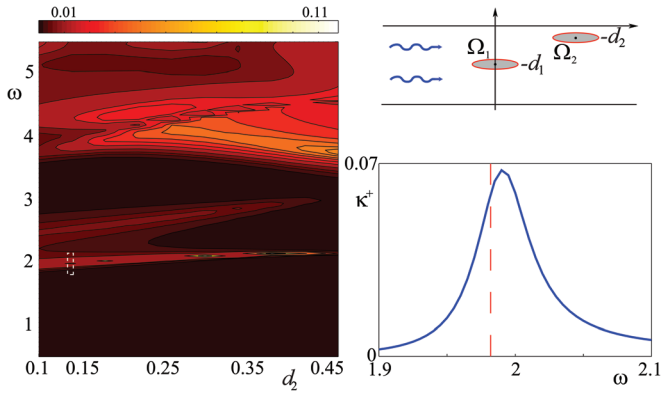


FIG. 5. (Color online) The transmission coefficient  $\kappa^+$  for two elliptic rigid inclusions as a function of the depth  $d_2$  and the frequency  $\omega$  (left) and a zoomed cut for  $d_2 = 0.14$  (right bottom).

vicinity of  $\omega \approx 1.985$ . This growth indicates the presence of a complex spectral point  $\omega_n$  not far from this frequency in spite of the fact that no spectral point exists in this range with a single rigid inclusion.

To check up this guess, the eigenfrequencies  $\omega_n^{FEM}$  and the eigenforms  $\mathbf{u}_n(x, z)$  of a finite-length specimen cut out from the infinite waveguide with the elliptic inclusions have been calculated using a finite element method (FEM). The nearest to the range of interest eigenfrequencies and eigenforms of the vertical displacement component  $|u_{z,n}(x, z)|$  are shown in Fig. 6. Among them, only the eigenform associated with the natural frequency  $\omega = 1.982$  is featured by a high oscillation amplitude between the inclusions. Namely this eigenfrequency is very close to the peak frequency  $\omega_p = 1.985$  in Fig. 5.

The concentration of oscillation between the obstacles is a sign of wave energy localization in this zone in the case of infinite waveguide. It differs from the situation with one inclusion when vortices appear in front of the obstacle [Fig. 2(b)]. With two and more obstacles, the vortices, appearing between them at resonance frequencies, start working not as blockers but as pumps. They let an energy flux pass through the defected zone rounding the vortex areas. The trajectory of resonance energy passing is clearly visible in Fig. 7, which gives examples of energy streamlines and power density distribution for the elastic layer with three thin rigid inclusions ( $l = 0.3$ ,  $d = 0.3$ ,  $\Delta x = 4$ ) at the nonresonance blocking frequency  $\omega = 0.98$  (top) and at the resonance “open up” frequency  $\omega_p = \text{Re}\omega_n = 1.15$  (bottom). In the power density subplot (d) the getting-through energy flux

goes along the piecewise-linear saw-shape gray path bouncing between the horizontal waveguide’s boundaries.

Thus, in the case of more than one obstacle, the nearly real spectral poles  $\omega_n$ , causing resonance wave transmission, may appear not only near the resonance gap ranges inherent for a single obstacle, as it was shown in the crack example above. They also appear in a nonresonance blocking range, where no poles are present with one obstacle as in the rigid inclusion examples. In the latter, the pass peaks pop up at the almost zero part of the  $\kappa^+(\omega)$  plot (Fig. 8). Moreover, those peaks look as twin peaks, indicating the presence of double poles located close to each other. Indeed, besides the pole  $\omega_1 = 1.150 - i0.009$ , which opens the waveguide at  $\omega_p = 1.15$  in Fig. 7, there exists one more nearby pole  $\omega_2 = 1.037 - i0.015$  yielding the left pass peak at  $\omega_p = 1.039$  (Fig. 8). Resonant pass peaks in the case of three cracks [Fig. 5(b) from Ref. 13] also look like twin peaks.

It should be mentioned that resembling pop-up appearance of pass peaks is inherent to 1D waveguide structure of various physical nature. For example, an unexpected resonant transmission peak appears in a gap band of a magneto-phonic structure combined of two ones separately possessing the full blocking abilities (Fig. 2 from Ref. 3).

### C. Multiple poles and resonant pass peaks

The study of resonance phenomena in 2D waveguides with multiple hidden defects (both cracks and inclusions) has revealed the following fact: the number of resonance poles  $\omega_n$  located near gap ranges increases in parallel with  $M$ . Subsequently, the number of high quality peaks indicating resonant transmission at the frequencies  $\omega_p \approx \text{Re}\omega_n$  also increases as  $M$  grows. As an example, Fig. 9 displays a series of plots  $\kappa^+(\omega)$  for different sets of the same thin rigid inclusions ( $l = 1$ ,  $d = 0.25$ ,  $\Delta x = 4$ ,  $M = 1, 2, \dots, 5$ ). The frequency range  $0.9 < \omega < 1.5$  in this series is taken narrower than in Fig. 8 to focus on the changes of pass peaks in one group. These plots are supplemented by Table I that displays the pass-frequencies  $\omega_p$  [i.e., the points of  $\kappa^+(\omega)$  local maxima], the spectral points  $\omega_n$  obtained from characteristic equation (2), and the eigenfrequencies  $\omega_n^{FEM}$  found using FEM for finite specimens cut out from the infinite waveguide. The real parts of  $\omega_n$  are also shown in the figure by arrows. The curves in the subplots of Fig. 9 and the values presented in Table I are in good agreement confirming the conclusion made about the role of resonance poles in the waveguide opening up.

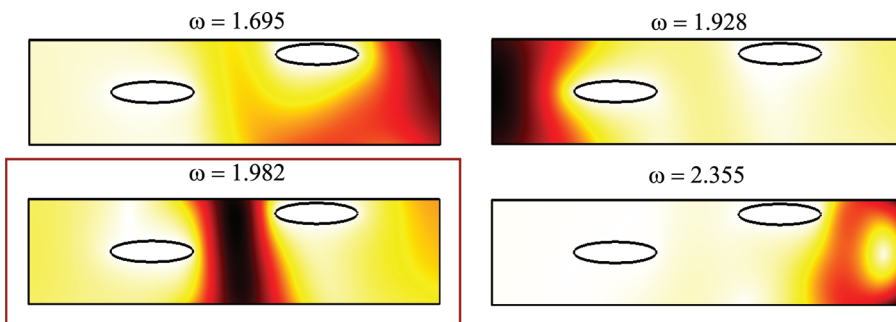


FIG. 6. (Color online) Eigenfrequencies and eigenforms  $|u_{z,n}(x, z)|$  of a finite elastic specimen with two rigid elliptic inclusions.

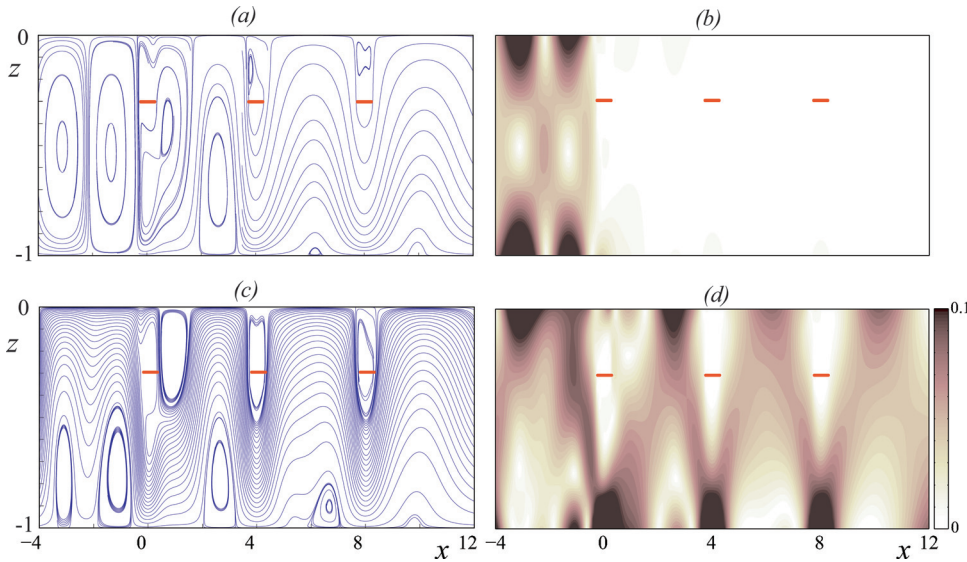


FIG. 7. (Color online) Energy streamlines (left) and power density  $|e(x, z)|$  (right) in the cases of nonresonant blocking (top) and resonant passing (bottom) by three thin rigid inclusions.

Similar connection between the allocation of spectral poles and comb-like patterns of transmission coefficient plots is known for 1D waveguides with multiple scatterers.<sup>8</sup> A close 1D analogous to the 2D waveguide considered is a spring supported string with pointwise defects. The derivation and analysis of the string solution, as well as the meaning of defect parameters, are particularized in Ref. 12. The frequency spectrum  $w(x, \omega)$  of vertical spring oscillation also has poles in the  $\omega$ -plane. Several examples of their distribution for periodic sets of defects are shown in Fig. 10. There are two types of defects spaced with the step  $\Delta x = 1$  and specified by the parameters  $\alpha_m = -0.5$  and  $\varepsilon_m = 0$  (top subplots) and  $\alpha_m = 0$  and  $\varepsilon_m = 10$  (bottom subplots). In the first set, negative values of the parameters  $\alpha_m$  decrease the string's cross section, hence the defects may be roughly treated as transverse cuts (cracks). In the second set, positive  $\varepsilon_m$  yield additional bending stiffness at the defect points, similar as in a layer with rigid inclusions.

The circle markers in the left subplots of Fig. 10 point out the pole location in the case of two defects ( $M=2$ ). For the defects of both types the poles go along the real axis with the period  $\text{Re}\omega_{n+1} - \text{Re}\omega_n \approx \pi/\Delta x$ , rising up to the axis as  $\text{Re}\omega_n$  increases, in the first case, and going down for the second set of defects. With a larger number of obstacles, the groups of  $M-1$  poles appear above these marked by circles places moving up closely to the real axis as  $M$  increases in

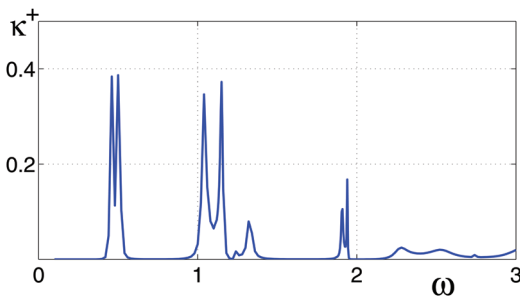


FIG. 8. (Color online) The transmission coefficient  $\kappa^+(\omega)$  for three rigid inclusions (as in Fig. 7) with popping up resonance peaks at  $\omega_p \approx \text{Re}\omega_n$ .

both cases. The right subplots demonstrate zoomed patterns of such pole groups for  $M=10, 20$  and  $40$  defects. In both cases they are arranged along arch-down curves that are pulled up to the axis as  $M \rightarrow \infty$ .

It is interesting that the arch-down pole patterns are practically the same as those shown in Figs. 1 and 2 from Ref. 8 for a 1D quantum system governed by the Schrödinger equation. Moreover, the poles obtained for 2D models (in particular, the poles given in Table I) also lie on arch-down curves.

In the first case ( $|\alpha_m| \neq 0$ , top subplots), the segments of the real axis, to which the pole groups approach, are separated by increasing intervals so that these bands shrink in

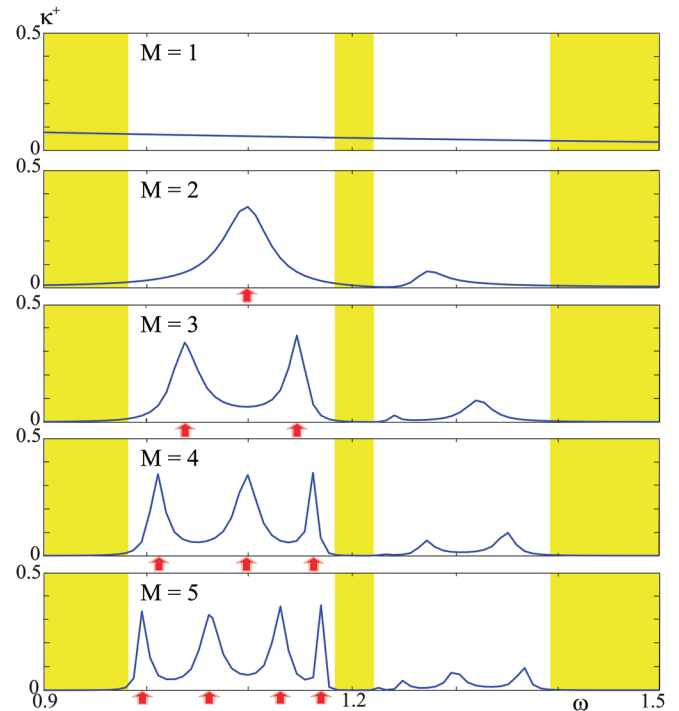


FIG. 9. (Color online) Appearance of additional resonant transmission peaks with increasing number of rigid inclusions  $M$ .

TABLE I. Pass frequencies  $\omega_p$ , complex spectral points  $\omega_n$ , and eigenfrequencies  $\omega_n^{FEM}$ .

M	$\omega_p$	$\omega_n$	$\omega_n^{FEM}$
2	1.100	$1.100 - 0.027i$	1.064
3	1.039	$1.037 - 0.015i$	1.008
	1.150	$1.150 - 0.009i$	1.115
4	1.012	$1.010 - 0.008i$	0.985
	1.101	$1.099 - 0.013i$	1.067
	1.166	$1.166 - 0.004i$	1.135
5	0.998	$0.997 - 0.004i$	0.972
	1.064	$1.063 - 0.010i$	1.032
	1.133	$1.132 - 0.008i$	1.099
	1.174	$1.173 - 0.002i$	1.143

points as  $\omega \rightarrow \infty$ . In the second case ( $\varepsilon_m \neq 0$ , bottom subplots), on the contrary, such bands increase as  $\omega \rightarrow \infty$  so that the intervals between them shrink in points.

The plots  $\kappa^+(\omega)$  for strings with  $M = 2, 5$ , and 20 defects of two selected types are shown in Fig. 11 by solid lines (the left and right subplots, respectively). The dashed curve at each subplot shows  $\kappa^+(\omega)$  for the case of the same single defect ( $M = 1$ ). It is clearly seen how the pass bands are formed out of the thickening sub-peaks centered just above the nearly real complex poles assembled in arch-down groups, as it is shown in Fig. 10. In accordance with the pole allocation the sub-peaks flood in the pass bands as  $M$  increases. With the infinite number of periodic defects ( $M = \infty$ ) the bounds of the pass and stop bands can be estimated using the Bloch-Floquet formalism.<sup>1</sup> As expected, it

has yielded the same bands as those obtained for large  $M$  within the model considered.

As mentioned above, similar transmission peaks have been observed for one-dimensional wave propagation in various structures with finite sets of obstacles. For example, the transmission plot given in Fig. 6 from Ref. 9 for a phononic lattice looks quite similar to the right subplots of Fig. 11. They are also composed of groups of multiple sub-peaks reaching the limiting value  $\kappa^+ = 1$ , the peaks in groups restricted from below by white arches and separated by strong stop bands. Though in the most known examples for waveguides with finite sets of scatterers, their spectral properties have not been analyzed, most likely, the pass and gap band phenomena in all these and many other cases described in acoustics and physics literature are also closely connected with the patterns of natural pole allocation.

As for the 2D elastic waveguides considered above, the transmission peaks located above the nearly real spectral poles  $\omega_n$  also form pass bands if the number of obstacles increases. In Fig. 9 the developing pass bands are shown by white background, while the shaded areas indicate remaining gap bands. As the main distinction from 1D waveguides, these peaks do not reach the maximal height  $\kappa^+ = 1$ , i.e., the resonance effect does not provide the full transmission in the case. The right pass band ( $1.25 < \omega < 1.4$ ) is associated with complex poles located more distantly from the real axis than those for the left band, that is why the related peaks are much smaller.

This distinction may ensue from the difference in the blocking-transmission mechanisms. In a 1D case it may be explained by the in-phase or anti-phase superposition of

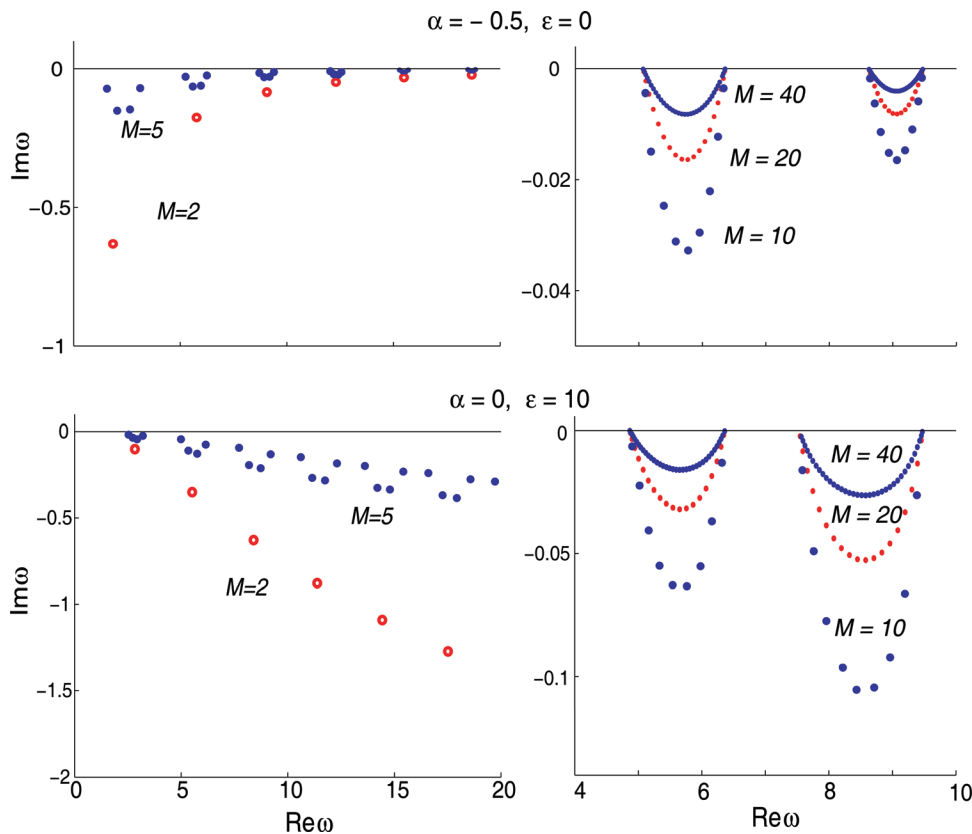


FIG. 10. (Color online) Allocation of nearly real poles  $\omega_n$  in the  $\omega$ -plane for  $M$  evenly spaced string defects.

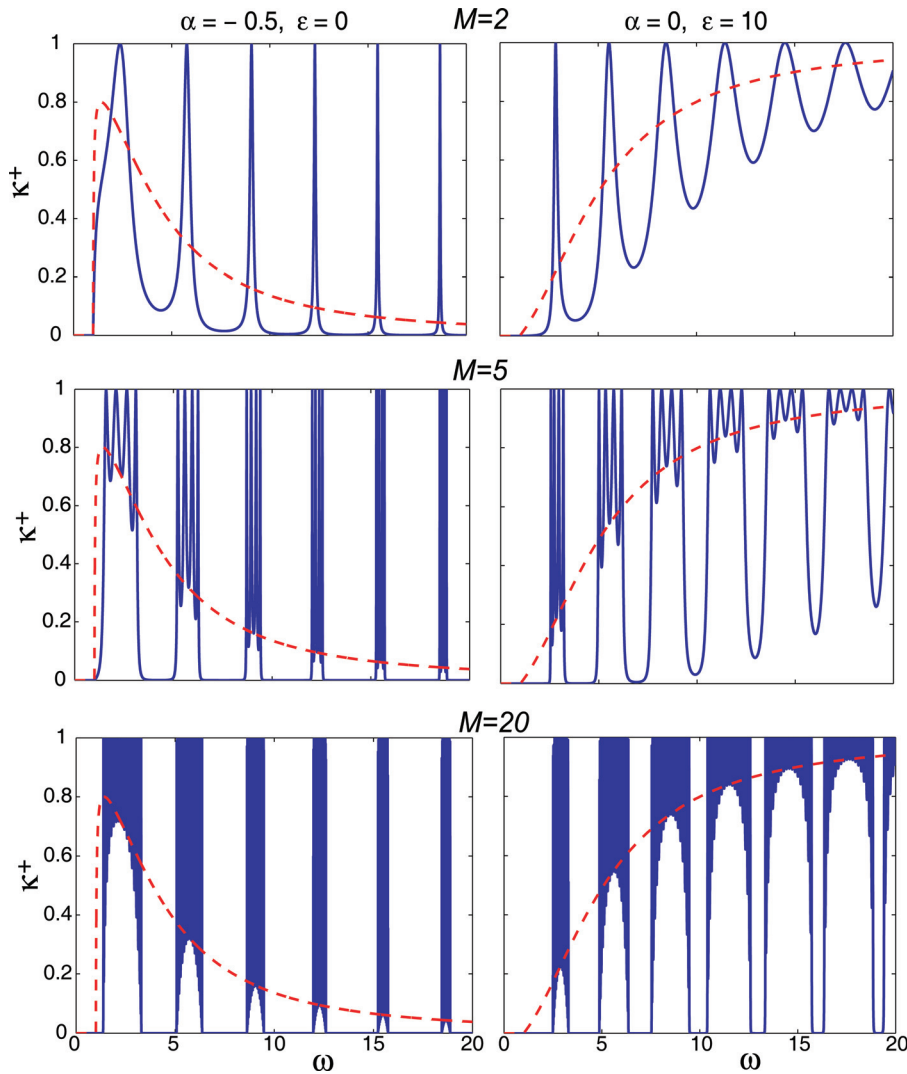


FIG. 11. (Color online) Plots  $\kappa^+(\omega)$  for wave transmission through  $M = 2, 5,$  and  $20$  string defects of the first (left) and second (right) kinds.

scattered waves enabling full transmission or full blocking, respectively. Hidden obstacles in a 2D waveguide do not interlap with its cross section, hence, certain wave fluxes passing around them may exist. Therefore, the mechanism cannot be reduced to a simple superposition of waves propagating straightforward along the layer. Instead, energy fluxes enveloping obstacles over fancy trajectories control these effects. With one obstacle, the resonance oscillation at a near-spectral frequency gives rise to large energy vortices shutting down the waveguide, while with multiple defects the resonance perturbation at  $\omega_p \approx \text{Re}\omega_n$  changes and realigns the vortex structure, opening up the waveguide in a narrow band.

It should be mentioned that some 2D waveguides may exhibit resonance patterns inherent to 1D ones. For example, the plots of transmitted energy flux ratio for Lamb wave propagation in an elastic layer with periodic rectangular sections of different material properties<sup>16</sup> show bands of multiple full transmission peaks alternating with full stop bands, just as in Fig. 11 for the string model. Unlike to cracks and inclusions, here the inhomogeneities completely dam up the cross section and the pass-block effects appear the same way as in a 1D defected string.

## V. CONCLUSION

Based on the analysis of wave transmission through defected zones in 2D elastic waveguides and of the allocation of natural resonance poles  $\omega_n$  in the complex frequency plane, the following inferences can be made:

- (1) with single-obstacle waveguides the appearance of nearly real spectral points  $\omega_n$  is featured by blocking effects accompanied by the wave energy localization in the form of energy vortices
- (2) with multiple obstacles the gap bands associated with every separate obstacle are joined together, but a high-quality resonant transmission takes place at the pass frequencies  $\omega_p \approx \text{Re}\omega_n$  inside the blocked ranges, just as in the case of 1D wave propagation; the trajectories of passing fluxes go around the energy vortices appearing near the obstacles
- (3) if the number of defects  $M \geq 2$ , the nearly real poles  $\omega_n$ —and thus the pass peaks above them—assemble in groups; as  $M$  increases, the poles concentrate within finite frequency ranges and the related pass peaks develop into pass bands.

## ACKNOWLEDGMENTS

This work is supported by the Russian Ministry for Education and Science projects ADTP 2.1.1/10463 and FTP 14.740.11.0578.

- <sup>1</sup>L. Brillouin, *Wave Propagation in Periodic Structures* (McGraw-Hill, New York, 1946) 247 p.
- <sup>2</sup>A. L. Chen and Y. S. Wang, "Study on band gaps of elastic waves propagating in one-dimensional disordered phononic crystals," *Physica B* **392**, 369–378 (2007).
- <sup>3</sup>T. Goto, A. V. Dorofeenko, A. M. Merzlikin, A. V. Baryshev, A. P. Vinogradov, M. Inoue, A. A. Lisyansky, and A. B. Granovsky, "Optical Tamm states in one-dimensional magnetophotonic structures," *Phys. Rev. Lett.* **101**, 113902 (2008).
- <sup>4</sup>A. V. Lavrinenko, W. Wohlleben, and R. J. Leyrer, "Influence of imperfections on the insulating and guiding properties of finite Si-inverted opal crystals," *Opt. Express* **17**(2), 747–760 (2009).
- <sup>5</sup>F. Ursell, "Trapping modes in the theory of surface waves," *Math. Proc. Cambridge Philos. Soc.* **47**, 347–358 (1951).
- <sup>6</sup>D. V. Evans and C. M. Linton, "Trapped modes in open channels," *J. Fluid Mech.* **225**, 153–175 (1991).
- <sup>7</sup>E. Glushkov, N. Glushkova, M. Golub, and A. Boström, "Natural resonance frequencies, wave blocking, and energy localization in an elastic half-space and waveguide with a crack," *J. Acoust. Soc. Am.* **119**(6), 3589–3598 (2006).
- <sup>8</sup>F. Barra and P. Gaspard, "Scattering in periodic systems: from resonances to band structure," *J. Phys. A* **32**(18), 3357–3375 (1999).
- <sup>9</sup>M. Sigalas, M. S. Kushwaha, E. N. Economou, M. Kafesaki, I. E. Psarobas, and W. Steurer, "Classical vibrational modes in phononic lattices: theory and experiment," *Z. Kristallogr.* **220**, 765–809 (2005).
- <sup>10</sup>D. W. L. Sprung, H. Wu, and J. Martorell, "Scattering by a finite periodic potential," *Am. J. Phys.* **61**(12), 1118–1124 (1993).
- <sup>11</sup>D. J. Griffiths and C. A. Steinke, "Waves in locally periodic media," *Am. J. Phys.* **69**(2), 137–154 (2001).
- <sup>12</sup>E. Glushkov, N. Glushkova, and J. Wauer, "Wave propagation in an elastically supported string with point-wise defects: Gap-band and pass-band effects," *Z. Angew. Math. Mech.* **91**(1), 4–22 (2011).
- <sup>13</sup>E. V. Glushkov, N. V. Glushkova, M. V. Golub, and Ch. Zhang, "Resonance blocking of traveling waves by a system of cracks in an elastic layer," *Acoust. Phys.* **55**(1), 8–16 (2009).
- <sup>14</sup>Ye. V. Glushkov, N. V. Glushkova, A. A. Yeregin, and V. V. Mikhas'kiv, "The layered element method in the dynamic theory of elasticity," *J. Appl. Math. Mech.* **73**, 449–456 (2009).
- <sup>15</sup>N. A. Umov, "The equations of motion of the energy in bodies [in Russian]," Odessa (1874), in: *Selected Works* (State Publishers of Technical-Theoretical Literature, Moscow-Leningrad, 1950); as cited by O. A. Godin, *J. Acoust. Soc. Am.* **125**(4), 1960–1970 (2009), and by A. P. Kiselev, *J. Math. Sci.* **19**(4), 1372–1375.
- <sup>16</sup>V. Pagneux and A. Maurel, "Lamb wave propagation in inhomogeneous elastic waveguide," *Proc. R. Soc. London* **458**, 1913–1930 (2002).